S1 Details for thermochronometric dating

S1.1 Finding outlier single grains of (U-Th)/He dating

The entire (U-Th-Sm)/He dataset of our analysed apatite and zircon single grains can be found in Tables S1 and S2, respectively. Calculating sample cooling ages for AHe and ZHe from the analysed single-grain ages was complicated for two main reasons. Cooling ages for the sedimentary rocks from the Olympic Mountains can be unreset, i.e., the single-grain ages can exhibit different age representative of the sediments' source terrains. Furthermore, the geologic uncertainty for (U-Th-Sm)/He dating is often larger than the analytic uncertainty, which could lead to overdispersed single grain ages (e.g. Fitzgerald et al., 2006; Flowers and Kelley, 2011). In order to determine whether this is the case for our samples or whether outliers are present, we proceeded as follows. Samples, of which single-grain ages are all older than the depositional age of the sample or of which single-grain ages show a large spread and do not overlap within analytical uncertainty (e.g., apatites of sample OP1560 or zircons of sample OP1557; Table S1 and S2), are considered as unreset samples. If samples pass this first test, we identify possible outliers by checking whether single-grain ages overlap within 2SD. Anomalously old single grains are considered outliers and excluded from sample cooling age calculations (e.g., single apatites of samples OP1552 and OP1553; Table S1). Furthermore, if single-grain ages of a sample are disputable, we consider information from the higher closure temperature system of the sample or other samples collected along the same elevation transect. For example, if the ZHe age of a certain sample is reset or if AHe ages of samples at higher or lower elevation have concordant ages, we consider the AHe system of that sample to be reset. This applies to AHe ages of samples OP1555, OP1572 and

OP1576. For samples OP1572 and OP1576, we take the youngest apatite single grain age as sample cooling age (due to the low high-quality apatite yield).

S1.2 Further information for FT dating

Data tables containing the information about the single grains used for fission-track dating of apatite and zircon are reported in Table S3 and S4.

S2 Additional information for creation of the sediment cross sections

For calculation of the sedimentary cross sections (Figure 7 in main paper), the lower boundary of the area occupied by the sediments corresponds to the top of the subducted slab, which is derived from the Slab1.0 model (Hayes et al., 2012; McCrory et al., 2012). Unfortunately, no uncertainty estimates are provided for their model, so we are not able to provide uncertainties for our lower boundary estimate. McCrory et al. (2012) only note, that their current estimate of the top of the subducted slab locally differs by 5 km (in the vertical dimension) from results from prior studies. But because the current study is the most comprehensive and up to date one, we use their results for our calculations.

The upper boundary is defined by the topography/bathymetry or the Hurricane Ridge Fault (HRF), a major discontinuity separating the accreted sediments from the overlying Coast Range Terrane (CRT). At the surface, the location of the HRF is taken from a geologic map (Tabor and Cady, 1978) and at depth we use information provided by a seismic study (Calvert et al., 2011). This study provides seismic velocities at depths of 22 km and 34 km for the Olympic Peninsula (Figure 3b and c in the original publication of Calvert et al., 2011), where a distinct area of low seismic velocities (LVZ = low velocity zone) can be observed beneath the Olympics. Calvert et al. (2011)

interpret this LVZ to correspond to accreted/underplated sediments, which are enclosed by material of higher seismic velocities (e.g., the subducted oceanic crust below or basaltic rocks of the CRT on top of the sediments).

Therefore, we assume that the eastern boundary of the LVZ represents the HRF and contour the boundary between low and high velocities for the depths of 22 km and 34 km. According to Calvert et al. (2011), the seismic velocities of the accreted sediments vary with latitude and range from 5.8–6.5 km/s (between 47.25°N and 48.1°N) and 6.7–7.0 km/s (north of 48.1°N). Hence, we mapped and contoured the boundary between sediments and CRT, distinguished by different velocities. The solid black line in Figure S1 is constructed using a seismic velocity of ~6.6 km/s (boundary between yellow and orange pixels in the original publication's figures), and we consider the volumes calculated with this outline as the most representative estimates. The cross sections and volumes shown in Figure 7 correspond to this geometry (yielding values of 5348 km^2 and 3672 km^2 for Profile 1 and 2, respectively).

In order to provide an uncertainty for our calculated volumes, we also provide outlines for the HRF using different velocities. A maximum extent uses a velocity of ~7.0 km/s as boundary between sediments and CRT (between bright and dark orange pixels), and a minimum extent uses a velocity of ~6.4 km/s as boundary (between light green and yellow). These maximum and minimum extents of the sediment are shown as thin, dashed lines in Figure S1 for the respective depths of 22 km and 34 km. The uncertainties in the location for the HRF reported in Figure 7 are based on these maximum and minimum extents. Volumes calculated with these extents yield values of 5186 km^2 and 5572 km^2 (Profile 1), and 3446 km^2 and 4005 km^2 (Profile 2). The uncertainties reported

for the calculated sediment reported in Figure 7 of the main manuscript are derived from these minimum/maximum extents, and correspond to 5–10% of the reported volume. Interestingly, the uncertainties on the location of the HRF at depth are largest in the southern part of the Olympic Peninsula (i.e., the width of the dashed lines around the thick, solid line in Figure S1). However, Calvert et al. (2011) also note, that the resolution of their reconstruction is disturbed on the northern part of the peninsula, where velocities for the accreted sediments could be higher compared to areas in the south. Hence, we hesitate to construct a cross section for this part of the mountain range.

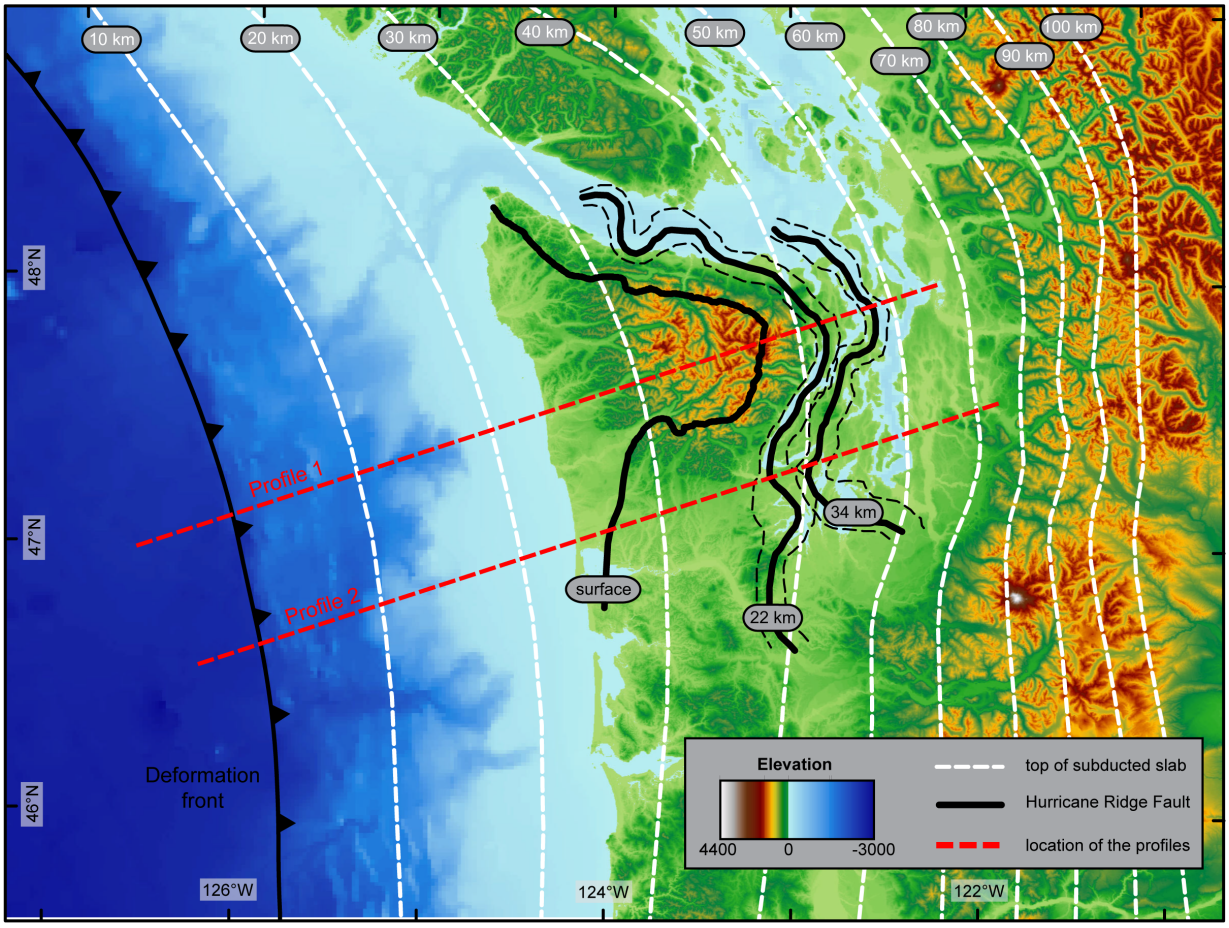

Figure S1: Map showing the data used for constructing Profile 1 and 2 (shown in Figure 7 of the main manuscript). Top of the subducted slab is taken from the Slab1.0 model (Hayes et al., 2012; McCrory et al., 2012). Outline of the Hurricane Ridge Fault is derived from a geologic map (Tabor and Cady, 1978) and at depth the contours are interpreted from the seismic study of (Calvert et al., 2011). See text for details.

References

Calvert, A. J., Preston, L. A. and Farahbod, A. M.: Sedimentary underplating at the Cascadia mantle-wedge corner revealed by seismic imaging, Nat. Geosci., 4(8), 545–548, doi:10.1038/ngeo1195, 2011.

Fitzgerald, P. G., Baldwin, S. L., Webb, L. E. and O'Sullivan, P. .: Interpretation of (U–Th)/He single grain ages from slowly cooled crustal terranes: A case study from the Transantarctic Mountains of southern Victoria Land, Chem. Geol., 225(1–2), 91–120, doi:10.1016/j.chemgeo.2005.09.001, 2006.

Flowers, R. M. and Kelley, S. A.: Interpreting data dispersion and "inverted" dates in apatite (U–Th)/He and fission-track datasets: An example from the US midcontinent, Geochim. Cosmochim. Acta, 75(18), 5169–5186, doi:10.1016/j.gca.2011.06.016, 2011.

Hayes, G. P., Wald, D. J. and Johnson, R. L.: Slab1.0: A three-dimensional model of global subduction zone geometries, J. Geophys. Res. Solid Earth, 117(B1), doi:10.1029/2011JB008524, 2012.

McCrory, P. A., Blair, J. L., Waldhauser, F. and Oppenheimer, D. H.: Juan de Fuca slab geometry and its relation to Wadati-Benioff zone seismicity, J. Geophys. Res. Solid Earth, 117(B9), doi:10.1029/2012JB009407, 2012.

Tabor, R. W. and Cady, W. M.: The structure of the Olympic Mountains, Washington: Analysis of a subduction zone, US Govt. Print. Off., 1978.